Strong Improvement of Long-Term Chemical and Thermal Stability of Plasmonic Silver Nanoantennas and Films

Xiaolong Wang, Christian Santschi, and Olivier J. F. Martin*

Silver (Ag) nanostructures and thin films are advantageous plasmonic materials as they have significantly lower losses than gold (Au). Unfortunately, Ag nanostructures suffer from poor chemical and thermal stability, which limit their applications. Here, the mechanisms leading to the deterioration of Ag nanostructures are clarified. It is first shown that oxygen alone cannot oxidize Ag nanostructures. Then, experiments using X-ray photoelectron spectroscopy reveal that the amount of sulfur in ambient air is too low for efficient tarnishing of the Ag surface. Finally, water is found to be the most critical factor for the degradation of Ag nanostructures and thin films. At high relative humidity, adsorbed water forms a thin film enabling the migration of Ag ions at the Ag/air interface, which deteriorates the Ag nanostructures. A dehydration treatment is developed which alters the morphology of the deposited silver, leading to an improved chemical and thermal stability of the Ag nanostructures and films, which then remain stable for more than 14 weeks under ambient laboratory conditions. In addition, dehydration also improves significantly the root-mean-square roughness for Ag thin films deposited on a glass substrate.

1. Introduction

Silver (Ag) is an appealing plasmonic material, since it exhibits significantly lower losses than gold (Au), especially for wavelengths below 500 nm.[1] Together with lower losses, Ag also provides a stronger field enhancement at the vicinity of plasmonic nanostructures and holds the promise of extending—together with aluminum—the spectral range where plasmonics can be used for many applications.[2–37] Au remains, however, the most popular plasmonic material due to its superior chemical and thermal stability compared to other materials.[38–41] Indeed, Ag is prone to degradation, which represents a significant drawback for long-term utilization. The deterioration of Ag is a well-known phenomenon that was intensively investigated a few decades ago.[42–47] It was shown that Ag nanoparticles (AgNPs) can be rapidly tarnished with a plasmonic resonance shift of 1.8 nm h^{-1} due to sulfur (S) contamination (sulfidation) in ambient laboratory air.[48–50] The role played by oxidation instead of sulfidation for Ag nanoparticles deterioration under normal ambient conditions was also evidenced.[51–54] Furthermore, it has been shown that both sulfidation and oxidation require water to take place.[55,56] To slow down the chemical deterioration of AgNPs, protective coating layers, including graphene,[57] SiO_2,[58–61] and organic thiol molecules,[62] were proposed. Furthermore, Ag thin films and nanoparticles are thermally unstable at elevated temperatures—even far below the melting point, such as the temperatures used for photoresist baking sequences—and, as a consequence, Ag nanostructures lose their specific plasmonic properties during those processes. The specific environment and substrate also determine this thermal stability,[63–67] aluminum doping and Ni/Ag(Al) alloying of Ag films also increase the thermal stability of Ag.[68,69] While here we focus on nanofabricated Ag structures, which shape can be designed at will, we should like to mention the large body of work on chemically synthesized crystalline Ag nanoparticles, which remain stable in solution as long as they are protected with capping agents.[70]

To improve roughness of an Ag film, different seed layers,[71–73] aluminum doping,[68] and template stripping

X. Wang, Dr. C. Santschi, Prof. O. J. F. Martin
Nanophotonics and Metrology Laboratory
Swiss Federal Institute of Technology (EPFL)
CH-1015 Lausanne, Switzerland
E-mail: christian.santschi@epfl.ch

DOI: 10.1002/smll.201700044

methods[74–77] have been developed. However, adhesion and seed layers increase the damping of a plasmonic system and, consequently, broaden the linewidth of the plasmon resonance.[78,79] Unfortunately, all these workarounds alter the optical properties of the nanostructures and, consequently, designs have to be adjusted in order to maintain the desired properties. An efficient stabilization scheme that would enable the routine utilization of silver nanostructures is therefore missing.

In this work, we demonstrate such a stabilization scheme and first show that oxygen (O_2) only does not deteriorate Ag nanostructures since Ag nanostructures exposed to pure O_2 maintain their optical and morphological properties. We then evidence, using X-ray photoelectron spectroscopy (XPS) technique that the concentration of sulfur in ambient air is far too low for a significant alteration of Ag nanostructures. We conclude that relative humidity (RH), forming adsorbed water layers, plays a key role in Ag degradation and we finally develop a dehydration process that dramatically improves the chemical and thermal stability of plasmonic Ag nanostructures and thin films.

2. Results and Discussion

2.1. Ag Antennas Deterioration over a Short Period of Time

Figure 1 shows fresh four-nanorod Ag antennas (4-NRSAs) fabricated using electron beam lithography (EBL) with subsequent thermal evaporation of Ag and lift-off process (see the Experimental Section for details on the fabrication). The 4-NRSA structure is chosen because of its strong Fano resonance, which is very sensitive to the shape of the nanostructure.[80] A gradual deterioration of the 4-NRSAs upon exposure to ambient conditions is clearly visible in Figure 1. Their morphology, examined using scanning electron microscope (SEM) and their optical properties, measured by dark-field scattering spectra (DFSS) are completely changed over that short period of time.

The fresh 4-NRSAs, as shown in Figure 1a, have good shapes and their DFSS (red curve in Figure 1e) agrees very well with the calculations (dashed lines in Figure 1e–h) using the surface integral equation (SIE) method.[81,82] The spectra exhibit a typical asymmetric Fano lineshape with a dip at the wavelength of $\lambda = 640$ nm (calculations) and $\lambda = 645 \pm 5$ nm (measurements). After exposure to ambient conditions for 2 d, the corresponding DFSS (green curve in Figure 1f) is blue shifted with respect to the original resonance (Figure 1e, red curve) and the Fano dip becomes less significant but is still clearly visible. After a 4 d storage period under ambient conditions, the morphology of the 4-NRSAs becomes quite fuzzy (Figure 1c) and the spectrum is further blue-shifted (Figure 1g). After 7 d of exposure, the original nanostructure morphology is completely lost (Figure 1d) and the Fano dip vanishes entirely (Figure 1h).

2.2. Deterioration Mechanisms of Ag Nanostructures and Films

The fact that O_2 causes Ag oxidation and eventually destroys Ag nanostructures is a widespread paradigm that is also supported by the literature.[51] To determine the exact role of O_2 in the deterioration mechanisms of Ag, two samples with 4-NRSAs on a glass substrate were fabricated and stored separately for two weeks in two different environments, O_2 and argon (Ar)—an inert gas in which Ag nanostructures

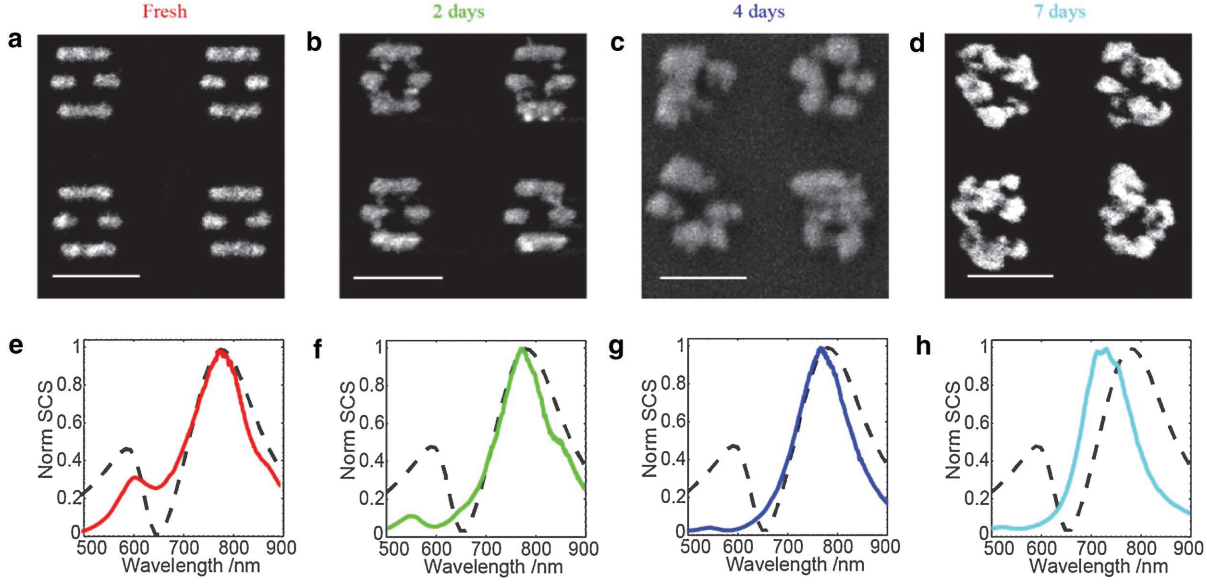

Figure 1. a) SEM image of the fabricated fresh 4-NRSAs. SEM images of the fabricated 4-NRSAs under ambient condition after b) 2, c) 4, and d) 7 d. e–h) Scattering spectra measured with dark-field spectroscopy corresponding to the SEM images (a)–(d). The dashed black curve represents the calculated scattering spectrum for the designed 4-NRSA. A single 4-NRSA consists of two long rods (length 130 nm) surrounding two short rods (length 68 nm). Width and height are 40 nm for all elements and the gaps between the rods are 30 nm. The Fano resonance dip is located at $\lambda = 640$ nm. The scale bars in (a)–(d) are 200 nm.

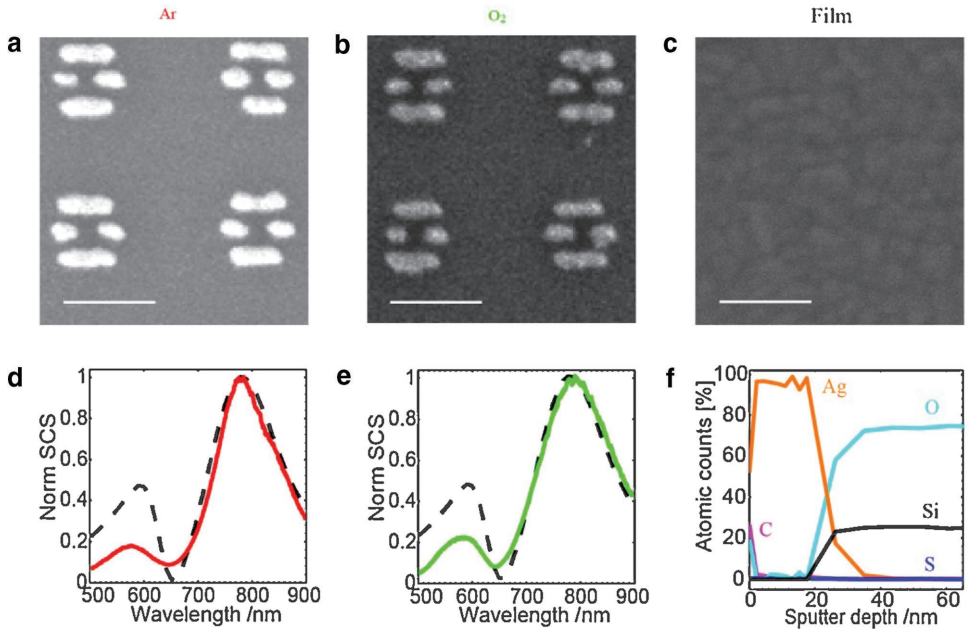

Figure 2. Morphology and optical properties of 4-NRSAs exposed to Ar and O_2. a) SEM of the 4-NRSAs exposed to Ar. b) SEM of the 4-NRSAs exposed to O_2. d,e) DFSS corresponding to (a) and (b). The dashed black represents the scattering spectrum of 4-NRSA calculated with SIE. c) SEM of Ag film stored in ambient air for two months. f) XPS analysis of specific elements in the Ag film shown in (c); the atomic concentrations of different elements are represented by the following colors: Ag: orange; O: cyan; Si: black; C: pink; and S: dark blue. The scale bars in (a)–(c) are 200 nm.

should not be altered. For reasons that will become obvious later, these experiments were performed under almost zero relative humidity. **Figure 2**a,b shows a comparison of the corresponding shapes of the 4-NRSAs stored under O_2 and Ar environments and Figure 2d,e displays the corresponding DFSS. Quite surprisingly, the morphology of the two 4-NRSAs does not show any changes over this relatively long time period, as was the case for the nanostructures exposed to ambient air reported in Figure 1b. The dip position in the asymmetric Fano lineshape remains at $\lambda = 645 \pm 5$ nm (red and green curves in Figure 2d,e) and is still in good agreement with the calculations (dashed black curve). These observations indicate that O_2 alone does not deteriorate the Ag nanostructures.

It has been proposed that atmospheric sulfur present in the air could produce Ag sulfidation and tarnish Ag nanostructures, leading to a resonance shift of 1.8 nm h^{-1}.[48] However, even in rural areas, the total concentration of atmospheric sulfur compounds is as low as a few ppb.[83] To clarify the effect of S, we stored a 40 nm thick Ag film under ambient conditions in the laboratory for two months and did not observe any degradation due to sulfidation, Figure 2c. The subsequent XPS analysis of this film, shown in Figure 2f, indicates that the atomic concentration of S (blue curve in Figure 2f) is extremely low, close to zero. We therefore conclude that sulfidation is not key to the deterioration of Ag, at least under laboratory conditions.

Since O_2 alone does not seem to deteriorate AgNPs, the influence of other parameters needs to be considered. Actually, it has been shown that both sulfidation and oxidation require adsorbed water to take place.[55,56] Ion release from AgNPs in aqueous environment is also known and has been studied in ecotoxicological contexts.[84,85] Finally, in a previous paper we have shown that water present during the evaporation significantly deteriorates the quality of nanoantenna made of aluminum (Al).[86] For these reasons, we address here the role of water in the deterioration of Ag nanostructures and perform experiments under two different RH conditions, namely, at 100% and under Ar atmosphere corresponding to near zero RH. To this end, two 4-NRSAs samples on a glass substrate were stored in recipients with low (almost 0%) and 100% RH for two weeks. For the low and high RH experiments the glass containers were dehydrated at 200 °C for 1 h and then stored in a dry Ar environment before the samples were introduced and the recipients subsequently sealed. In the high RH experiment a vial filled with water, to ensure 100% RH, was additionally introduced into the recipient prior to sealing. The results are shown in **Figure 3**.

Figure 3a,b shows the shapes of the 4-NRSAs exposed to two different RH. The 4-NRSAs survive under low RH while they are completely ruined and lose their shape under 100% RH. The asymmetric Fano lineshape obtained by DFSS maintains its dip at $\lambda = 635 \pm 5$ nm (Figure 3c) for low RH, still in good agreement with the calculation (dashed black curve). On the other hand, the DFSS completely loses its asymmetric Fano lineshape when the 4-NRSAs are stored at 100% RH under Ar atmosphere. These results clearly demonstrate that humidity or adsorbed water is absolutely indispensable for the deterioration of Ag nanostructures.

The formation of small nanoparticles scattered around the main body of the 4-NRSA and forming a near circular shape (Figure 3b) is caused by the surface migration of ionic Ag in adsorbed water.[56,87] Keast et al. reported that the small particles arising from the parent particles consist of Ag_2S and are formed by the dominating process of sulfidation.[87] Since in our previous experiment no S was detected, such a mechanism can be excluded here.

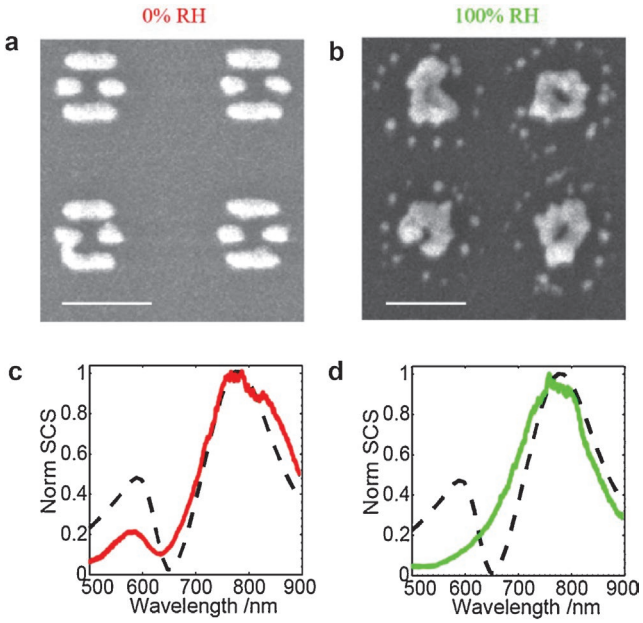

Figure 3. Morphology and optical properties of 4-NRSAs exposed for two weeks to a,c) 0% and b,d) 100% RH. a,b) SEM images and c,d) corresponding DFSS (the dashed black curve represents the scattering spectrum of the 4-NRSA calculated with SIE). The scale bars in (a) and (b) are 200 nm.

Measurements of adsorbed water using attenuated total reflection (ATR) infrared spectroscopy have revealed the existence of three RH-dependent regimes of adsorbed water.[88] At low, intermediate, and high RH, well-ordered ice-like, quasi-liquid, respectively, liquid configurations are formed. It has been proposed that metallic Ag° can be oxidized to Ag^+ in the presence of dissolved O_2 and water according to the following reaction:[84]

$$2Ag^0 + \frac{1}{2}O_{2(aq)} + 2H^+_{(aq)} \rightarrow 2Ag^+_{(aq)} + H_2O \quad (1)$$

Dissolution of metal into ionic Ag enables migration in the adsorbed liquid water layer, which explains the degradation of the Ag nanostructures at high HR and the formation of satellites around its main body, as shown in Figure 3b. On the other hand, at low RH the reverse reaction of (1), reaction (2) prevails, which reduces ionic Ag into a more stable configuration which suppresses migration efficiently:

$$2Ag^0(\text{stable}) + \frac{1}{2}O_{2(aq)} + 2H^+_{(aq)} \leftarrow 2Ag^+_{(aq)} + H_2O \quad (2)$$

Motivated by these observations and the atomic force microscopy (AFM) measurements described below, we have developed the dehydration process described in the next section to prevent the deterioration of Ag nanostructures.

2.3. Dehydration to Chemically Stabilize Ag Nanostructures

We again fabricated 4-NRSAs on glass substrates as shown in **Figure 4**a. The shape of fresh 4-NRSAs and the corresponding DFSS are displayed in Figure 4a,d. The 4-NRSAs were then stored in a chamber continuously purged with dry Ar gas to remove adsorbed water from the surface of the 4-NRSAs (see the Experimental Section for details). After that, the sample was removed from the chamber and stored under ambient condition at a RH of 45 ± 2% (measured with HYGROLOG-HL-NT3 monitor). The shape and optical properties of the nanostructures were monitored every two weeks up to 14 weeks. Figure 4 shows some SEM images with corresponding DFSS (the full information on morphology and optical properties up to 14 weeks is provided in Figure S1, Supporting Information). From Figure 4a,c it can be seen that, following the dehydration process, the shape of 4-NRSAs did not change significantly, although the samples were stored under ambient condition. Furthermore, the corresponding DFSS still maintain their asymmetric Fano lineshape as shown in Figure 4d,f. These results clearly demonstrate the improved stability for the Ag nanostructures, also under ambient conditions.

2.4. Dehydration to Thermally Stabilize Ag Nanoantenna

As demonstrated and in agreement with literature,[56,87] humidity—or, better, adsorbed water—induces spontaneous Ag^+ migration and the nondehydrated Ag nanostructures lose rapidly their original shape at temperatures well below the melting point (see **Figure 5**b), at, for example, 180 °C, which is the pre/post-photoresist baking temperature for standard e-beam lithography. Although the melting point for bulk Ag is 893 °C,[89] the nondehydrated 4-NRSAs already lose their shape after 5 min baking on a hot plate in air at 180 °C, Figure 5b. Consequently, the asymmetric Fano resonance is also modified by the baking process, as can be seen when comparing Figure 5d and 5e. On the other hand, both, the shape and the DFSS of the dehydrated 4-NRSAs are preserved after the baking process, Figure 5c,f. We conclude that during the dehydration process the Ag morphology is changed through reactions (1) and (2) from an unstable to a more stable morphology which is also indicated by the AFM measurements shown in **Figure 6**. The deposition process leaves the silver in an unstable morphology. From this morphology, under ambient conditions, the silver nanostructures can easily deteriorate. Under a dry Ar environment, adsorbed H_2O is significantly reduced, Ag^+ migration efficiently suppressed and, according to reaction (2), the silver is transformed into a more stable morphology.

2.5. Dehydration to Thermally Stabilize and Improve the Surface Roughness of Ag Films

Like their nanostructure counterparts, thin Ag films have also a poor thermal stability.[63,64,66,67,90] To investigate the thermal stability of Ag films at elevated temperature (180 °C, far below the melting point though), 40 nm thick Ag films were thermally evaporated on glass substrates (for details see the Experimental Section). Figure 6a shows a typical SEM image of such a thin film. The first sample was

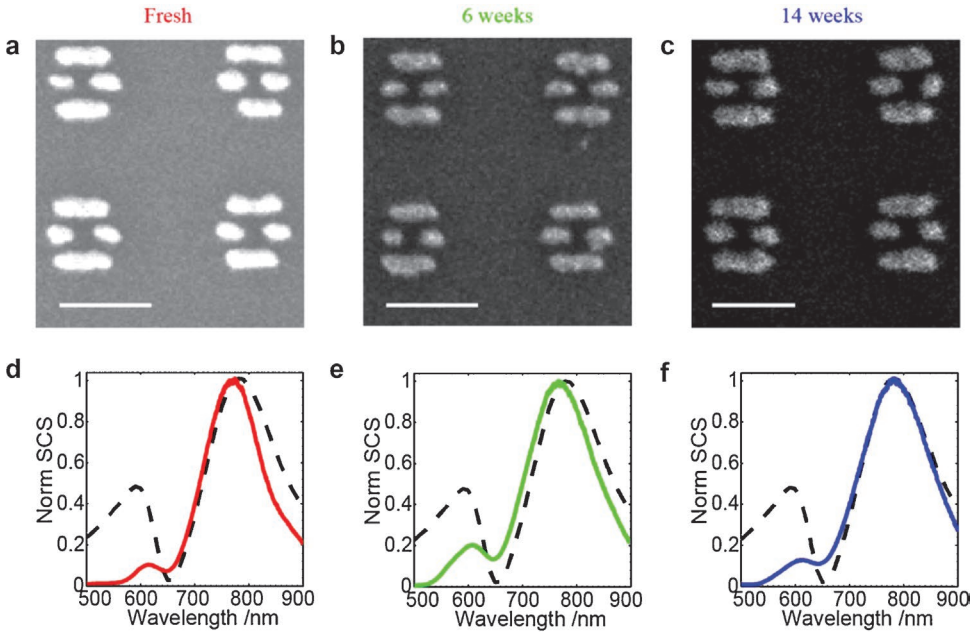

Figure 4. Temporal tracking of morphology and optical properties of the 4-NRSA over a long period of time (14 weeks). a) SEM image of the freshly fabricated 4-NRSA. b) SEM image of the dehydrated 4-NRSA after six weeks stored under ambient condition. c) SEM image of the dehydrated 4-NRSA after 14 weeks stored under ambient condition. d–f) DFSS corresponding to (a)–(c). The dashed black curve corresponds to the scattering spectrum of the 4-NRSA calculated with SIE. The scale bars in (a)–(c) are 200 nm.

baked 5 min on a hot plate at 180 °C in air. After such a treatment the film became discontinuous and islands were formed (Figure 6b). The other sample was first dehydrated as described previously (Figure 6c) and then baked for 5 min on a hot plate at 180 °C in air (Figure 6d). Comparing with the nondehydrated sample reveals a very significant improvement of the film thermal stability (compare Figure 6b and 6d).

AFM measurements were performed for these samples and the results are shown in Figure 6e–h. Figure 6i–l shows the peak-to-valley height (PTVH) profile in the center of the films marked by the black line in Figure 6e–h.

The PTVH amplitude for the fresh film is larger than for the dehydrated film, compare Figure 6i and 6k. The PTVH amplitude for the dehydrated then baked film remains smaller than for the fresh one, compare Figure 6l and 6i.

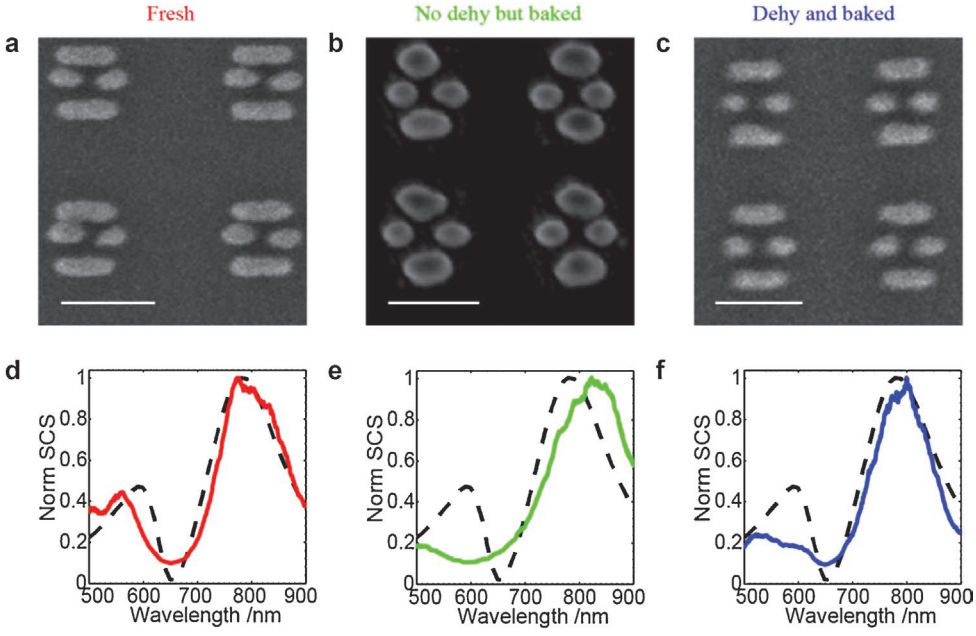

Figure 5. Morphology and optical properties of baked 4-NRSA with and without previous dehydration process. a) SEM image of freshly fabricated fresh 4-NRSA. b) SEM image of 4-NRSA baked without previous dehydration. c) SEM image of the 4-NRSA baked after dehydration. d–f) DFSS corresponding to (a)–(c). The dashed black curve is the scattering spectrum of the 4-NRSA calculated with SIE. The scale bars in (a)–(c) are 200 nm.

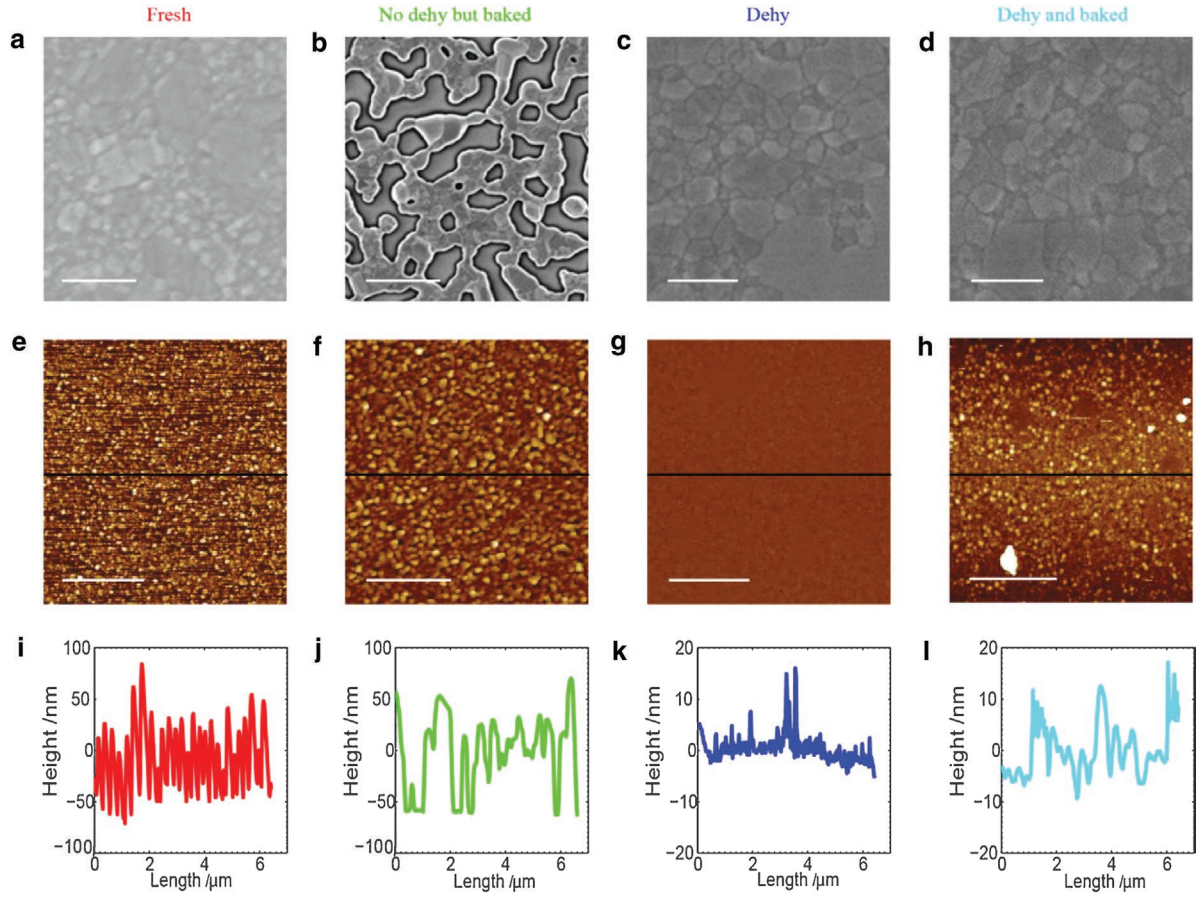

Figure 6. Morphology of baked films with and without dehydration. SEM images of Ag films a) freshly deposited and b) after baking, without dehydration. SEM images of Ag film c) after dehydration and d) after subsequent baking. e–h) AFM images of the deposited Ag films corresponding to the SEM images (a)–d). i–l) Corresponding peak-to-valley height profiles along the black lines marked in the AFM images (e)–(h). The scale bars in (a)–(d) are 200 nm and the scale bars in (e)–(h) are 2 μm.

Calculating the surface roughness root mean square (RMS) of all the films, we observe that for a nondehydrated film the RMS is increased from 29.9 to 40.4 nm during the baking process (Figure 6xe,f). After dehydration the RMS decreases from 29.9 to 2.8 nm (Figure 6e,g) and then slightly increases to 6.6 nm after baking (Figure 6h). This is a further indication that dehydration leads to a reorganization of the thin Ag films according to reactions (1) and (2) and results in a more stable configuration for thin Ag films. This observation points in the interesting direction of studying the stability of Ag nanostructures from the perspective of crystallinity; it is possible that a monocrystalline Ag nanostructure is very stable and also exhibits exceptional optical properties, as is the case for Au nanostructures.[91]

3. Conclusions

It has been evidenced that the deterioration of Ag nanostructures and films is closely linked to the presence of surface-adsorbed water. The chemical and thermal stability of Ag nanostructures and thin films can be strongly enhanced by a dehydration process using a constant Ar flow. This dehydration dramatically reduces the migration process (with water as catalyst) of ionic Ag, which is essentially responsible for the deterioration of Ag. The dehydrated 4-NRSAs shapes were geometrically optically stable for 14 weeks. After dehydration, both 4-NRSAs and films survive baking processes at 180 °C. Furthermore, the surface RMS roughness of Ag film was improved from 29.9 to 2.8 nm after dehydration. This study paves the way for the fabrication of Ag nanostructures and thin films that are chemically and thermally stable under ambient conditions for a broad range of applications, including in the short wavelength and near-UV ranges of the spectrum.

4. Experimental Section

Ag Antenna Fabrication: The Ag 4-NRSA fabrication combines standard EBL, thermal evaporation of metallic thin film, and lift-off processes. Thin glass substrate (D263 SCHOTT AG, 150 μm thick 4 in. wafer was diced to produce square chips with size 20 mm × 20 mm) was cleaned with acetone and isoproplyl alcohol (IPA). Two layers of polymethyl methacrylate (PMMA, from Microresist Technology GmbH) with a mass of 495 kDa (thickness of 120 nm) followed by a layer of 950 kDa (thickness of 60 nm) were spun-coated. Each layer was pre/post-baked 5 min at 180 °C. A 20 nm chromium layer was evaporated on top of the resist (Leybold Optics LAB600H) serving as a conducting layer for the e-beam exposure. The 4-NRSAs were patterned with EBL (Vistec EBPG5000

system) using a 100 keV electron beam (current 200 pA). Subsequent chromium etching (30 s) and followed by development (60 s) in a mixture of MiBK solution and IPA was performed. An oxygen plasma for 8 s (O_2: 300 sccm, RF power: 500 W, pressure: 2 Torr, Oxford PRS900 dry etcher) removed the remaining residues of the e-beam resist and activated the surface of the substrate. A 40 nm Ag film was evaporated using the same evaporator as for Cr with a different recipe as detailed by Thyagarajan.[86] Finally, a lift-off process in acetone was performed for 1 d and the sample was subsequently washed and dried with IPA and nitrogen, respectively.

Ag Film Preparation: The 40 nm Ag film was evaporated using the recipe as the deposited film for the antenna on a cleaned glass substrate (D263 SCHOTT AG, thickness of 150 µm wafer diced in chips of 20×20 mm^2).

Characterization: The SEM images of the 4-NRSAs were recorded using a Zeiss Merlin field emission scanning electron microscope (Carl Zeiss Jena GmbH) at 2 keV. The scattering spectra were measured with a homemade white light (a halogen lamp) illumination and dark-field microscope (Olympus I $\times$ 71 with a PLAPON 60$\times$ oil immersion 1.45 NA objective). A polarizer (LPVIS050-MP, Thorlabs) was used to set the polarization along the axes of the long rod of the 4-NRSA. The structures were immersed in deionized (DI) water allowing use of high NA objective. The scattered light was measured with a spectrometer (Shamrock SR-303i, Andor) connected to a CCD camera (iDUS 401BRDD, Andor).

Atomic Force Microscope: The topography of the Ag films was characterized using a FastScan AFM (Bruker GmbH) in tapping mode with a silicon tip at ambient condition. The RMS roughness was calculated based on the peak-to-valley height difference from the topology data.

XPS Analysis: The XPS analysis was performed using a PHI VersaProbe II model from Physical Instruments AG, Germany. The elements analysis of the Ag film was performed using a monochromatic Al Kα X-ray source with 24.1 W power with a beam size of 100 µm and the binding energy was calibrated with C 1s value at 187.85 eV. The depth profile was measured by recording the XPS spectrum of the top surface and subsequent Ar^+ (2 keV) ion beam sputtering. The atomic concentration of Ag, Si, C, O, and S was calculated from the integrated intensity of the Ag 3d, Si 2p, C 1s, O 1s, and S 2p peaks for each depth.

Dehydration Process: The 4-NRSAs and thin films were stored in 2 in. single wafer carriers (TED PELLA, Inc.) after fabrication. The samples were then transferred into a DRY KEEPER (Sato Keiryoki MFG CO. LTD) which was purged continuously with Ar gas at 20 °C 1.013 Pa pressure and 5 nL min^{-1} for three weeks.

Simulation Methods: The SIE method was used to numerically compute the scattering spectrum of the 4-NRSAs.[92] For silver, a realistic dielectric function was taken (Johnson and Christy)[93] and the surrounding refractive index was set to 1.33 to approximately compensate the substrate-induced frequency shift for nanoparticle plasmon resonances.[94]

Supporting Information

Supporting Information is available from the Wiley Online Library or from the author.

Acknowledgements

The authors acknowledge the technical support from the Molecular and Hybrid Materials Characterization Center (MHMC EPFL), especially Dr. Pierre Mettraux for XPS analysis. The authors are grateful to Patrick Madliger and Jean-Marie Voirol for supporting the dehydration setup. The authors thank Dr. T. V. Raziman for insightful comments on the manuscript and support with the numerical calculations. This work was supported by funding from the European Research Council (ERC-2015-AdG-695206 Nanofactory).

Conflict of Interest

The authors declare no conflict of interest.

[1] P. R. West, S. Ishii, G. V. Naik, N. K. Emani, V. M. Shalaev, A. Boltasseva, *Laser Photonics Rev.* **2010**, *4*, 795.
[2] A. V. Akimov, A. Mukherjee, C. L. Yu, D. E. Chang, A. S. Zibrov, P. R. Hemmer, H. Park, M. D. Lukin, *Nature* **2007**, *450*, 402.
[3] P. Berini, I. De Leon, *Nat. Photonics* **2012**, *6*, 16.
[4] J. H. Park, P. Ambwani, M. Manno, N. C. Lindquist, P. Nagpal, S.-H. Oh, C. Leighton, D. J. Norris, *Adv. Mater.* **2012**, *24*, 3988.
[5] A. A. High, R. C. Devlin, A. Dibos, M. Polking, D. S. Wild, J. Perczel, N. P. de Leon, M. D. Lukin, H. Park, *Nature* **2015**, *522*, 192.
[6] S. V. Jayanti, J. H. Park, A. Dejneka, D. Chvostova, K. M. McPeak, X. Chen, S.-H. Oh, D. J. Norris, *Opt. Mater. Express* **2015**, *5*, 1147.
[7] V. J. Sorger, N. Pholchai, E. Cubukcu, R. F. Oulton, P. Kolchin, C. Borschel, M. Gnauck, C. Ronning, X. Zhang, *Nano Lett.* **2011**, *11*, 4907.
[8] B. Y. Zheng, Y. Wang, P. Nordlander, N. J. Halas, *Adv. Mater.* **2014**, *26*, 6318.
[9] L. Zhou, C. Zhang, M. J. McClain, A. Manjavacas, C. M. Krauter, S. Tian, F. Berg, H. O. Everitt, E. A. Carter, P. Nordlander, N. J. Halas, *Nano Lett.* **2016**, *16*, 1478.
[10] R.-H. Fan, R.-W. Peng, X.-R. Huang, J. Li, Y. Liu, Q. Hu, M. Wang, X. Zhang, *Adv. Mater.* **2012**, *24*, 1980.
[11] K. M. McPeak, C. D. van Engers, S. Bianchi, A. Rossinelli, L. V. Poulikakos, L. Bernard, S. Herrmann, D. K. Kim, S. Burger, M. Blome, S. V. Jayanti, D. J. Norris, *Adv. Mater.* **2015**, *27*, 6244.
[12] S. H. Lee, T. W. Johnson, N. C. Lindquist, H. Im, D. J. Norris, S.-H. Oh, *Adv. Funct. Mater.* **2012**, *22*, 4439.
[13] Z. Fang, X. Zhu, *Adv. Mater.* **2013**, *25*, 3840.
[14] Y. Wu, M. Gong, M.-C. Lin, C. Yuan, M. Angell, L. Huang, D.-Y. Wang, X. Zhang, J. Yang, B.-J. Hwang, H. Dai, *Adv. Mater.* **2016**, *28*, 9218.
[15] D. J. de Aberasturi, A. B. Serrano-Montes, L. M. Liz-Marzán, *Adv. Opt. Mater.* **2015**, *3*, 602.
[16] K. Sadecka, M. Gajc, K. Orlinski, H. B. Surma, A. Klos, I. Jozwik-Biala, K. Sobczak, P. Dluzewski, J. Toudert, D. A. Pawlak, *Adv. Opt. Mater.* **2015**, *3*, 381.
[17] Z. Feng, C. Jiang, Y. He, S. Chu, G. Chu, R. Peng, D. Li, *Adv. Opt. Mater.* **2014**, *2*, 1173.
[18] I. J. H. McCrindle, J. Grant, T. D. Drysdale, D. R. S. Cumming, *Adv. Opt. Mater.* **2014**, *2*, 149.
[19] S. Ye, X. Zhang, L. Chang, T. Wang, Z. Li, J. Zhang, B. Yang, *Adv. Opt. Mater.* **2014**, *2*, 779.
[20] M. R. Gartia, A. Hsiao, A. Pokhriyal, S. Seo, G. Kulsharova, B. T. Cunningham, T. C. Bond, G. L. Liu, *Adv. Opt. Mater.* **2013**, *1*, 68.
[21] V. E. Ferry, J. N. Munday, H. A. Atwater, *Adv. Mater.* **2010**, *22*, 4794.
[22] V. K. Valev, J. J. Baumberg, C. Sibilia, T. Verbiest, *Adv. Mater.* **2013**, *25*, 2517.

[23] H. M. Chen, C. K. Chen, M. L. Tseng, P. C. Wu, C. M. Chang, L.-C. Cheng, H. W. Huang, T. S. Chan, D.-W. Huang, R.-S. Liu, D. P. Tsai, *Small* **2013**, *9*, 2926.
[24] V. Giannini, A. I. Fernández-Domínguez, Y. Sonnefraud, T. Roschuk, R. Fernández-García, S. A. Maier, *Small* **2010**, *6*, 2498.
[25] Z. Fang, Y. Wang, C. Liu, S. Chen, W. Sang, C. Wang, J. Zeng, *Small* **2015**, *11*, 2593.
[26] Y.-J. Oh, S.-G. Park, M.-H. Kang, J.-H. Choi, Y. Nam, K.-H. Jeong, *Small* **2011**, *7*, 184.
[27] Y. Chen, N. Gao, J. Jiang, *Small* **2013**, *9*, 3242.
[28] W. Zhu, M. G. Banaee, D. Wang, Y. Chu, K. B. Crozier, *Small* **2011**, *7*, 1761.
[29] M. Thämer, A. Kartouzian, P. Heister, T. Lünskens, S. Gerlach, U. Heiz, *Small* **2014**, *10*, 2340.
[30] R. Gunawidjaja, E. Kharlampieva, I. Choi, V. V. Tsukruk, *Small* **2009**, *5*, 2460.
[31] Y. J. Li, X. Xiong, C.-L. Zou, X. F. Ren, Y. S. Zhao, *Small* **2015**, *11*, 3728.
[32] N. Liu, Z. Li, H. Xu, *Small* **2012**, *8*, 2641.
[33] I. Abdulhalim, *Small* **2014**, *10*, 3499.
[34] L. T. Varghese, L. Fan, Y. Xuan, C. Tansarawiput, S. Kim, M. Qi, *Small* **2013**, *9*, 3778.
[35] B. Yang, N. Lu, D. Qi, R. Ma, Q. Wu, J. Hao, X. Liu, Y. Mu, V. Reboud, N. Kehagias, C. M. S. Torres, F. Y. C. Boey, X. Chen, L. Chi, *Small* **2010**, *6*, 1038.
[36] Q. Chen, X. Hu, L. Wen, Y. Yu, D. R. S. Cumming, *Small* **2016**, *12*, 4922.
[37] C. T. Riley, J. S. T. Smalley, K. W. Post, D. N. Basov, Y. Fainman, D. Wang, Z. Liu, D. J. Sirbuly, *Small* **2016**, *12*, 892.
[38] W. A. Murray, W. L. Barnes, *Adv. Mater.* **2007**, *19*, 3771.
[39] Y. Jin, *Adv. Mater.* **2012**, *24*, 5153.
[40] M. W. Knight, N. S. King, L. Liu, H. O. Everitt, P. Nordlander, N. J. Halas, *ACS Nano* **2014**, *8*, 834.
[41] D. Nepal, K. Park, R. A. Vaia, *Small* **2012**, *8*, 1013.
[42] B. T. Reagor, J. D. Sinclair, *J. Electrochem. Soc.* **1981**, *128*, 701.
[43] J. M. Bennett, J. L. Stanford, E. J. Ashley, *J. Opt. Soc. Am.* **1970**, *60*, 224.
[44] J. L. Stanford, *J. Opt. Soc. Am.* **1970**, *60*, 49.
[45] H. E. Bennett, R. L. Peck, D. K. Burge, J. M. Bennett, *J. Appl. Phys.* **1969**, *40*, 3351.
[46] J. P. Franey, G. W. Kammlott, T. E. Graedel, *Corros. Sci.* **1985**, *25*, 133.
[47] T. E. Graedel, J. P. Franey, G. J. Gualtieri, G. W. Kammlott, D. L. Malm, *Corros. Sci.* **1985**, *25*, 1163.
[48] M. D. Mcmahon, R. Lopez, H. M. Meyer, L. C. Feldman, R. F. Haglund, *Appl. Phys. B* **2005**, *80*, 915.
[49] J. L. Elechiguerra, L. Larios-Lopez, C. Liu, D. Garcia-Gutierrez, A. Camacho-Bragado, M. J. Yacaman, *Chem. Mater.* **2005**, *17*, 6042.
[50] W. Cao, H. E. Elsayed-Ali, *Mater. Lett.* **2009**, *63*, 2263.
[51] T. W. H. Oates, M. Losurdo, S. Noda, K. Hinrichs, *J. Phys. D: Appl. Phys.* **2013**, *46*, 145308.
[52] W. M. Moore, P. J. Codella, *J. Phys. Chem.* **1988**, *92*, 4421.
[53] Y. Han, R. Lupitskyy, T.-M. Chou, C. M. Stafford, H. Du, S. Sukhishvili, *Anal. Chem.* **2011**, *83*, 5873.
[54] Q. Hua, A. Dimitri, G. Orest, S. M. Prokes, *Nanotechnology* **2010**, *21*, 215706.
[55] T. E. Graedel, *J. Electrochem. Soc.* **1992**, *139*, 1963.
[56] R. D. Glover, J. M. Miller, J. E. Hutchison, *ACS Nano* **2011**, *5*, 8950.
[57] J. C. Reed, H. Zhu, A. Y. Zhu, C. Li, E. Cubukcu, *Nano Lett.* **2012**, *12*, 4090.
[58] P. H. Smith, H. Gurev, *Thin Solid Films* **1977**, *45*, 159.
[59] D. Adams, T. L. Alford, *Mater. Sci. Eng., R* **2003**, *40*, 207.
[60] P. Benzo, L. Cattaneo, C. Farcau, A. Andreozzi, M. Perego, G. Benassayag, B. Pécassou, R. Carles, C. Bonafos, *J. Appl. Phys.* **2011**, *109*, 103524.
[61] H. Matthias, G. D. Di, E. Olivier, F. Christian, *Nanotechnology* **2007**, *18*, 015702.
[62] A. Desireddy, B. E. Conn, J. Guo, B. Yoon, R. N. Barnett, B. M. Monahan, K. Kirschbaum, W. P. Griffith, R. L. Whetten, U. Landman, T. P. Bigioni, *Nature* **2013**, *501*, 399.
[63] S. K. Sharma, J. Spitz, *Thin Solid Films* **1980**, *65*, 339.
[64] T. L. Alford, L. Chen, K. S. Gadre, *Thin Solid Films* **2003**, *429*, 248.
[65] C. E. Sanders, D. Verreault, G. S. Frankel, H. C. Allen, *J. Electrochem. Soc.* **2015**, *162*, C630.
[66] K. Thürmer, E. D. Williams, J. E. Reutt-Robey, *Phys. Rev. B* **2003**, *68*, 155423.
[67] H. C. Kim, T. L. Alford, D. R. Allee, *Appl. Phys. Lett.* **2002**, *81*, 4287.
[68] D. Gu, C. Zhang, Y.-K. Wu, L. J. Guo, *ACS Nano* **2014**, *8*, 10343.
[69] C. H. Chou, C. L. Lin, Y. C. Chuang, H. Y. Bor, C. Y. Liu, *Appl. Phys. Lett.* **2007**, *90*, 022103.
[70] B. Wiley, Y. Sun, B. Mayers, Y. Xia, *Chem. - Eur. J.* **2005**, *11*, 454.
[71] H. Liu, B. Wang, E. S. P. Leong, P. Yang, Y. Zong, G. Si, J. Teng, S. A. Maier, *ACS Nano* **2010**, *4*, 3139.
[72] V. J. Logeeswaran, N. P. Kobayashi, M. S. Islam, W. Wu, P. Chaturvedi, N. X. Fang, S. Y. Wang, R. S. Williams, *Nano Lett.* **2009**, *9*, 178.
[73] W. Chen, K. P. Chen, M. D. Thoreson, A. V. Kildishev, V. M. Shalaev, *Appl. Phys. Lett.* **2010**, *97*, 211107.
[74] P. Nagpal, N. C. Lindquist, S.-H. Oh, D. J. Norris, *Science* **2009**, *325*, 594.
[75] N. Vogel, J. Zieleniecki, I. Koper, *Nanoscale* **2012**, *4*, 3820.
[76] N. C. Lindquist, T. W. Johnson, D. J. Norris, S.-H. Oh, *Nano Lett.* **2011**, *11*, 3526.
[77] K. M. McPeak, S. V. Jayanti, S. J. P. Kress, S. Meyer, S. Iotti, A. Rossinelli, D. J. Norris, *ACS Photonics* **2015**, *2*, 326.
[78] T. Siegfried, Y. Ekinci, O. J. F. Martin, H. Sigg, *ACS Nano* **2013**, *7*, 2751.
[79] X. Jiao, J. Goeckeritz, S. Blair, M. Oldham, *Plasmonics* **2009**, *4*, 37.
[80] A. Lovera, B. Gallinet, P. Nordlander, O. J. F. Martin, *ACS Nano* **2013**, *7*, 4527.
[81] B. Gallinet, O. J. F. Martin, *Photonics Nanostruct. Fundam. Appl.* **2010**, *8*, 278.
[82] A. M. Kern, O. J. F. Martin, *J. Opt. Soc. Am. A* **2009**, *26*, 732.
[83] J. H. Seinfeld, S. N. Pandis, *Atmospheric Chemistry and Physics from Air Pollution to Climate Change: Problem Solution Manual*, Wiley, New York **1998**.
[84] J. Liu, R. H. Hurt, *Environ. Sci. Technol.* **2010**, *44*, 2169.
[85] Z.-M. Xiu, Q.-B. Zhang, H. L. Puppala, V. L. Colvin, P. J. J. Alvarez, *Nano Lett.* **2012**, *12*, 4271.
[86] K. Thyagarajan, C. Santschi, P. Langlet, O. J. F. Martin, *Adv. Opt. Mater.* **2016**, *4*, 871.
[87] V. J. Keast, T. A. Myles, N. Shahcheraghi, M. B. Cortie, *J. Nanopart. Res.* **2016**, *18*, 1.
[88] D. B. Asay, S. H. Kim, *J. Phys. Chem. B* **2005**, *109*, 16760.
[89] D. R. Lide, *Handbook of Chemistry and Physics: A Ready-Reference Book Chemical and Physical Data*, CRC Press, Boca Raton, FL, USA, **2000**.
[90] C. E. Sanders, C. Zhang, G. L. Kellogg, C.-K. Shih, *Surf. Sci.* **2014**, *630*, 168.
[91] J.-S. Huang, V. Callegari, P. Geisler, C. Brüning, J. Kern, J. C. Prangsma, X. Wu, T. Feichtner, J. Ziegler, P. Weinmann, M. Kamp, A. Forchel, P. Biagioni, U. Sennhauser, B. Hecht, *Nat. Commun.* **2010**, *1*, 150.
[92] T. V. Raziman, W. R. C. Somerville, O. J. F. Martin, E. C. Le Ru, *J. Opt. Soc. Am. B* **2015**, *32*, 485.
[93] P. B. Johnson, R. W. Christy, *Phys. Rev. B* **1972**, *6*, 4370.
[94] H. Fischer, O. J. F. Martin, *Opt. Express* **2008**, *16*, 9144.

Received: January 4, 2017
Revised: April 21, 2017
Published online: May 24, 2017